Journal of ELECTRONIC MATERIALS, Vol. 37, No. 4, 2008 Regular Issue Paper
DOI: 10.1007/s11664-007-0360-9
© 2007 TMS

Origin of Surface Defects in PCB Final Finishes by the Electroless Nickel Immersion Gold Process

BAE-KYUN KIM,[1,3] SEONG-JAE LEE,[1] JONG-YUN KIM,[1] KUM-YOUNG JI,[1] YEO-JOO YOON,[1] MI-YANG KIM,[1] SONG-HAE PARK,[1] and JONG-SOO YOO[2]

1.—Analytical Research Group, Corporate R&D Institute, Samsung Electro-mechanics Co., Ltd., 314, Maetan-3-dong, Yeoung-tong-ku, Suwon, Kyungki-do 443-743, South Korea. 2.—BGA Manufacturing Technology Group, BGA Division, Samsung Electro-mechanics Co., Ltd., 314, Maetan-3-dong, Yeoung-tong-ku, Suwon, Kyungki-do 443-743, South Korea. 3.—e-mail: baekyun.kim@samsung.com

We suggest a unique mechanism for surface defect generation causing solder joint or bonding failures in printed circuit boards (PCBs). Surface defects can be defined as corroded holes or spikes of the Ni-P layers on the soldering or wire bonding pads of PCBs. The typical defects are the black pad or pinhole pad defects generated after final finishing by the electroless nickel immersion gold (ENIG) process. Once corroded voids or spikes are plentifully created in nickel/gold interfaces, the bonding strength of solder or wire bonding joints is reduced. Therefore, it is important to characterize the details of these surface defects. In this paper, the defect microstructures and the P content variation with the ENIG processes are investigated. The surface defect selectivity with pad size and pad connectivity is suggested based on the key findings of P content variation. An overall mechanism is proposed based on a mixed mode of concentration cell corrosion and galvanic cell corrosion. Based on these results, more reasonable root causes are suggested.

Key words: Surface defects, black pad defects, electroless nickel immersion gold, final finishes, PCB, joint failures, hypercorrosion defects

INTRODUCTION

The Restriction of Hazardous Substances Directive (RoHS) issued by the European Union (EU) has been applied as a legal restriction since July 2006. Lead-free solder technology for printed circuit boards (PCBs) has therefore become an important issue due to these legal restrictions against environmentally hazardous materials. As a result, in the packaging industry, the study of connectivity between PCBs and lead-free solders has become a hot issue. In order to understand this connectivity, for example, for soldering or wire-bonding, details of the final finishes to PCBs should be addressed before understanding the interfaces between the PCB and solder after reflow soldering processes.

Electroless nickel/immersion gold plating (ENIG) processes are some of the most relevant surface treatments among the final finishing methods of PCBs. The reasons are that ENIG provides a coplanar surface suitable for both PCBs and printed wiring boards (PWBs) and also meets the requirements for lead-free package assembly.[1,2–5] Finishes by ENIG also provide a precious-metal contact surface that provides the excellent conductivity, wettability, and corrosion resistance of Au.[1,3–5] In general, an ENIG process consists of a series of consecutive unit processes: the acid cleaning, soft etching, acid pre-dip, activator treatment, electroless Ni plating, and immersion gold plating processes.[3,4] The two-layer metallic coating obtained from the ENIG processes includes nickel and gold

(Received March 8, 2007; accepted November 27, 2007; published online January 4, 2008)

layers between the metal finishing and solder balls or Au bonding wires. The nickel layers above the copper metallization on the PCBs play a barrier role against copper-gold interdiffusion. The top gold layers provide good wetting, the surface contact between the PCB surfaces and the Au bonding wires, and good electric conductivity.[6]

Surface defects on the pads can lead to severe failures in solder joints or wire bonding as they can lead to dewetting or nonwetting of non-lead solders or wires. These failures may result in poor quality and impact on PCB reliability.[2,3,7–11] PCB surface finishes using ENIG may cause solder joint detachment or an interfacial fracture of solder or wire bonding connections due to surface defects. Surface defects in an ENIG-treated PCB, so-called black pads, are known by various names: black-line nickel, black pads, black pad failure, black spot defect, or black pad defects.[1,5–11,12] Among these, since black-line nickel defects originate from nickel oxidation during the soldering processes, this defect type is beyond the scope of this paper, which deals with black pad defects originating from hyperactive corrosion in the Ni-P layer after the ENIG process.

During the immersion gold (IG) processes, it is known that hyperactive corrosion of the Ni plating occurs on the electroless nickel layer.[1,5–10,12] Numerous attempts have been made to demonstrate the root causes of bondability problems or solderability failures, and to understand the mechanism and the root causes of black pad defects.[1,5–9,11,12] Experimental data relating to process control factors such as phosphor contents, pH, temperature, and pad geometry in the nickel bath may help us to understand the mechanism of defect generation.[3,5–8] Reasonable root causes, however, have not been proposed. Despite numerous characterizations describing these defects, the overall mechanism and relationship between problematic process control factors have not been appropriately described. To understand failures of solder joints or wire bonding, details of the microstructures and defect characterization should be addressed. Details of the microstructural characterization can help us to understand the mechanism of the defect generation. Describing the microstructural details of these defects should be the first step towards establishing the mechanism and understanding the root causes.

In this paper, key findings after ENIG are precisely described and reported. The purpose of this paper is to suggest the main mechanism for the formation of black spot defects. Future work may address the defects' mechanism and their prevention in the final finishing process.

EXPERIMENTAL PROCESS

Prepared Samples

Samples that suffered from Au wire-bonding failures were examined as part of a microstructural investigation. To understand the black pad defects, other samples were independently prepared on a laboratory scale by the ENIG processes displayed in Fig. 1. The test, in which PCB coupons were fabricated by the above procedures, is illustrated schematically in Fig. 2. The numbers displayed in the pads are their areas in units of square millimeters. The pads surrounded by the solid lines are internally connected to each other as well as to the sides of the wire bonding and the solder pads. The wire bonding pads shown in Fig. 2 are categorized into two types: B-pads and G-pads. B-pads (indicating "bad pads") are connected internally to the wide gold finishing pad on the reverse side of the PCB: the large pad size is around 54.3 mm^2. G-pads (indicating "good pads") have no connection to each other or the reverse side of the pad. Many black pad

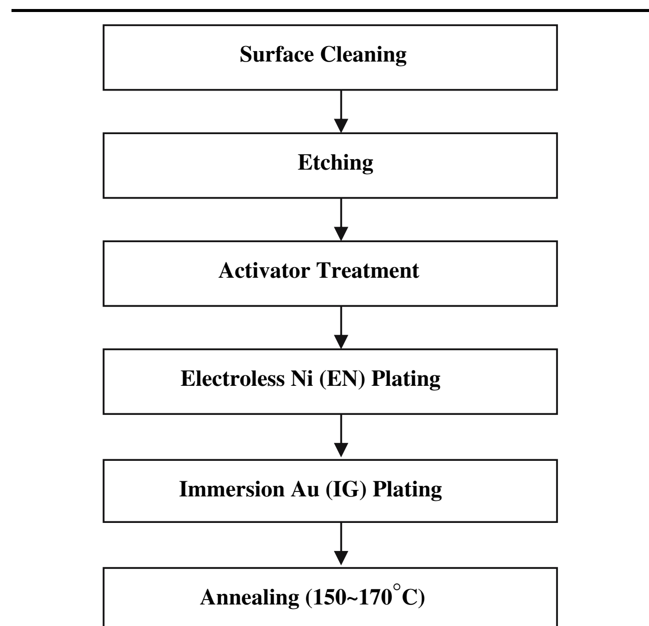

Fig. 1. The electroless nickel immersion gold (ENIG) process.

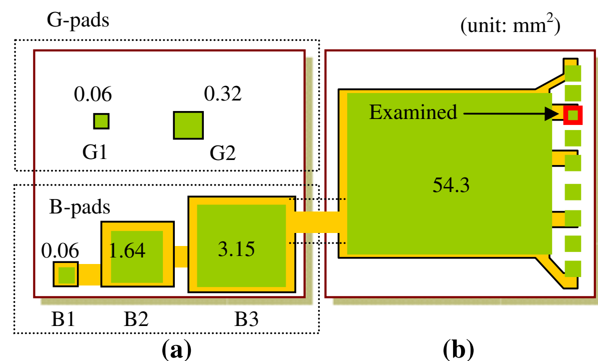

Fig. 2. Schematic PCB diagrams showing the pad arrangement of (a) the wire bonding pads and (b) the solder pads fabricated for the PCB test sample. The numbers displayed in the pads are their areas in units of square millimeters. The pads surrounded by solid lines are internally connected to each other as well as to the sides of the wire bonding pads and solder pads.

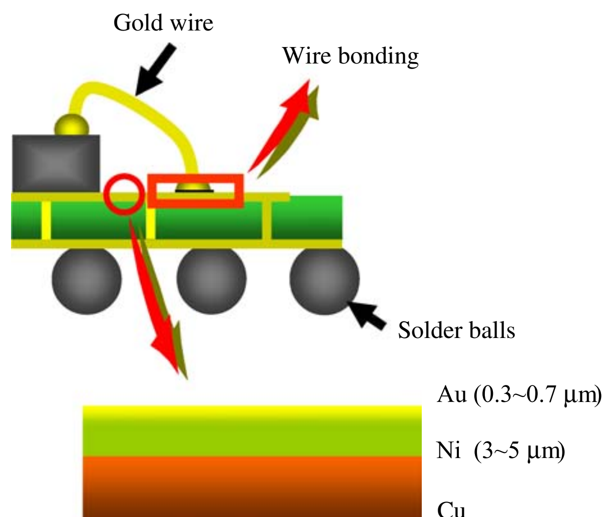

Fig. 3. Schematic PCB assembly structure showing final finishes (Au/Ni layers).

defects were found in the B-pads while fewer were found in the G-pads not connected to the large pads. The solder pad marked with an arrow in Fig. 2 and pad B1 were selected and examined for defect description by cross-sectioning based on focused ion beam milling (FIB). Figure 3 shows a schematic diagram of the PCB and the structure of the final finishing layers. The phosphor content of all the pads was also investigated and compared.

Characterization Methods

To examine the characteristics of the Ni layer surfaces after the ENIG process, a pretreatment is required. It is known that surface defects are generated during IG processes after EN processes.[1,5–10,12] For this pretreatment, a commercial KCN chemical solution was applied for one minute as a gold stripper. Cyanide has been used to strip off the gold layer without corrupting the Ni-P surfaces.[6,7] After removing the Au layer successfully, the nickel surfaces were cleaned with distilled water. After stripping the gold layers, the P content of the nickel layer surfaces was measured by a CAMECA SX100 electron probe microanalyzer (EPMA) under conditions of 15 kV, 10 nA, beam size (BS): 50 μm, and dwell time (DT): 0.2S or normal energy-dispersive X-ray spectroscopy (EDS). The phosphor content in the nickel layers is a good indicator of the degree of corrosion.[6,7,11] A linear correlation between percentage corrosion and phosphor content has been reported.[11] Phosphor enrichment of the nickel surface results from a decrease of nickel content due to corrosion of the surfaces of the Ni-P layers. Since nickel is corroded from the Ni-P layers after hypercorrosion, the increase of P content consequently takes place at the top surfaces of the Ni-P layers after the ENIG processes. Before and after gold stripping, microstructures were recorded by a field-emission scanning electron microscopy (FE SEM) at 20 kV. Cross-sectional microstructures were investigated by a Seiko SMI 2200, an FEI FIB 800, and a STRATA 400S. The conditions for the cross-sectioning by FIB were 30 kV and 93 pA.

RESULTS

Defect Description

Two types of surface defects were observed, as shown in Fig. 4: black pad (Fig. 4a) and pinhole pad (Fig. 4b) defects. In Fig. 4a, obtained from a wire bonding pad after Au wire bonding failure, the black areas at the nodule boundaries are indicated with solid arrows. These defects are likely to be the black pad defects widely known due to their dark discoloration. In the other sample that failed the bonding test, many pinholes (Fig. 4b) are observed in the bonding pads. Also, the pinhole defects are located at the nodule boundaries, as shown in Fig. 4b. This type of defect can be defined as a pinhole pad defect and is unlikely to be a black pad defect.

Figure 5 shows a cross-sectional view of the defect structures at the black-pad defective area illustrated in Fig. 4a. Corroded spike-like defects with narrow holes along the layer growth direction are observed. In the areas associated with the pinhole defect (Fig. 4b), the microstructure exhibits a similar structure as in the black pad defective areas. Figure 6 shows SE images and FIB micrographs. By serial sectioning, the rectangular area indicated in Fig. 6a was precisely investigated. Figure 6b–f shows this rectangular area cut off up to 520 nm along a direction parallel to the surface at a scale of hundreds of nanometers. The main spikes are connected to the deep nodule boundaries and the Au plating is opened along the main spike area. When it is appropriately cut off by FIB, each spike area is likely to connect directly to the open area of the Au plating layers.

As a result, we can conclude that both the black pad and pinhole pad defects have the same microstructure in spite of their different surface characteristics. In fact, the black color in the black pad defects is due to Ni atomic diffusion through the thin Au layer. Ni element traces are found on the Au

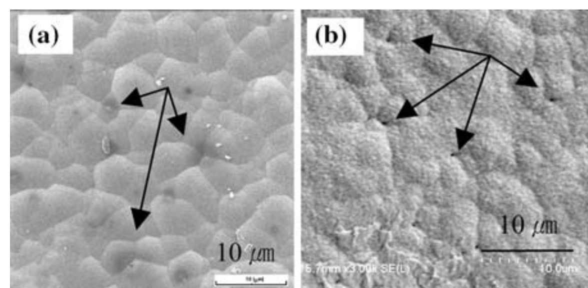

Fig. 4. Secondary electron (SE) micrographs demonstrating the types of surface defects observed: (a) black spots and (b) pinholes observed on Au surfaces after the ENIG processes.

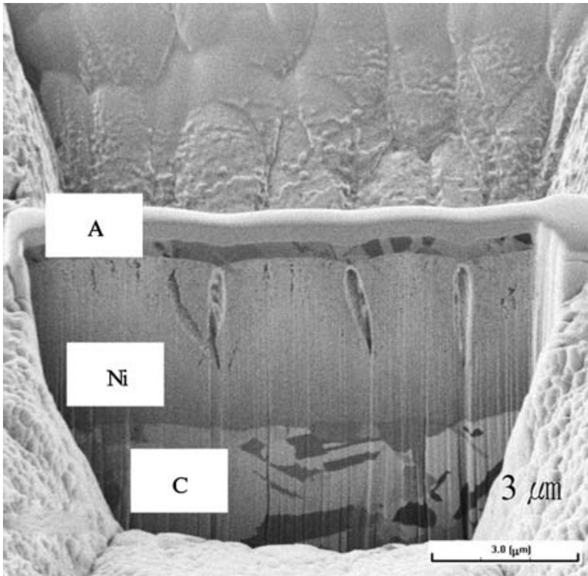

Fig. 5. Cross-sectional FIB image of the black spot area selected in the ball grid array (BGA) PCB. The microstructure shows the typical Au layer with a thickness of around 0.3 μm to 0.35 μm and the Ni layer with a thickness of 4 μm to 5 μm prepared by the ENIG processes.

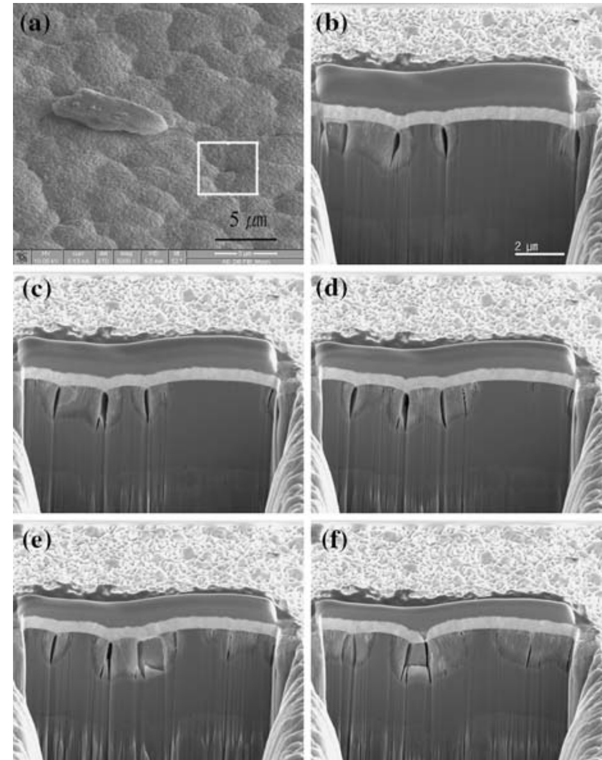

Fig. 6. (a) SE image showing pinholes at the Au surfaces after the ENIG processes and FIB images serially cross-sectioned along the direction parallel to the surface at a scale of hundreds of nanometers: (b) 0 nm, (c) 200 nm, (d) 300 nm, (e) 400 nm, and (f) 520 nm.

surfaces, as shown in Fig. 4a, but are absent in Fig. 4b. If Ni atomic diffusion takes place along the open Au plating area, the Au surfaces may look like Fig. 4a. These phenomena actually depend on the Au thickness. The sample used for Fig. 4a has a Au thickness of around 300 nm to 350 nm, whereas the Au thickness of the sample in Fig. 4b was around 550 nm to 600 nm, these values being estimated from the FIB micrographs (Figs. 5 and 6).

Phosphorous Content Variation with ENIG Processes

Figure 7 shows the surface microstructures of the B1 and G1 bonding pads with an area of 0.065 mm^2 after the EN processes. There are no major differences in nodule morphology or P content, as measured simply using an EDS in the SEM. After the ENIG processes, the surface microstructures of the same pads shown in Fig. 7 are shown in Fig. 8 with SE and backscattered electron (BSE) images. A BSE image enables compositional contrast imaging of the element: a dark area in a BSE image means that lighter elements or voids exist. In the B1 pad, the pinhole pad defects can be identified by comparing with the BSE micrograph of the G1 pad. The BSE image shown in Fig. 8b clearly shows dark circular spots and dark nodule boundaries.

After the ENIG processes, to examine the Ni layers, deposited Au layers were removed by using a gold stripper. The surface microstructure after stripping the gold layers is displayed in Fig. 9. The microstructure of the B1 pad is quite different to that of the G1 pad. The nodule boundaries in the B1 pad are more clearly displayed than in the G1 pad due to high boundary energy generated by hyper-

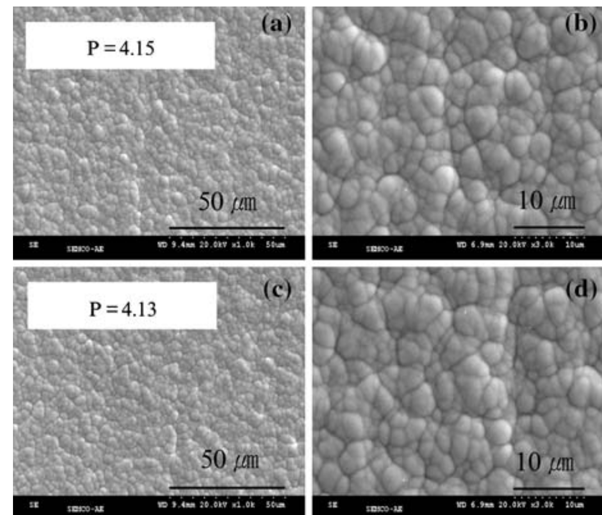

Fig. 7. SE micrographs of wire bonding pads with a size of 0.065 mm^2 belonging to the B-pads (a and b) and G-pads (c and d) after electroless Ni processes. The phosphor content was not different for the two pads.

corrosion of the Ni layers. It is worth noting that there is a large difference in the P content: 11.32 wt.% in the B1 pad compared to 4.25 wt.% in the G1 pad. In the G1 pad, the P content does not change before or after the IG processes, which

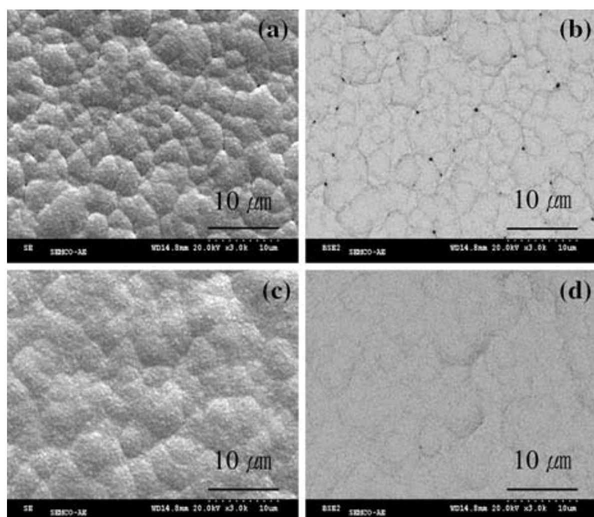

Fig. 8. Micrographs showing the surface microstructure of the pads in Fig. 5 after ENIG processes: (a) SE and (b) BSE images of the B1 pad, and (c) and (d) of the G1 pad.

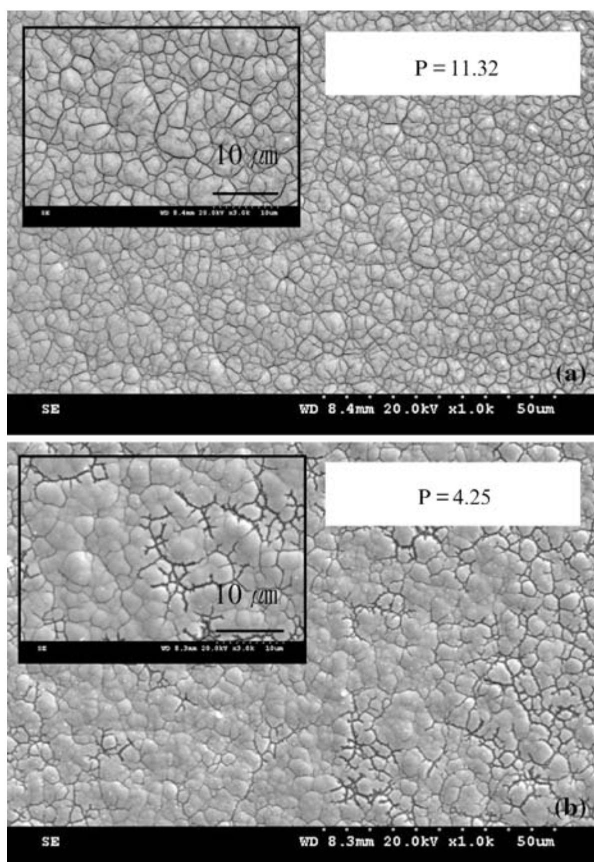

Fig. 9. SE micrographs showing the surface microstructure of the pads selected in Fig. 5 after the ENIG processes and Au stripping: (a) B1 and (b) G1 pads.

indicates that the B1 pad is severely corroded, as confirmed by the FIB cross-sectioned microstructure examination. It should also be noted that, based on the SEM micrograph results, the corrosion attack started at the nodule boundaries or junctions. These results coincide with previous results in the literature.[5] Additionally, it is noted that, despite the fact that the two pads have the same area, the tendency for defect generation varied with pad connectivity in the PCB. In this paper, connectivity means whether the pads connect to the large pad placed on the opposite side or not.

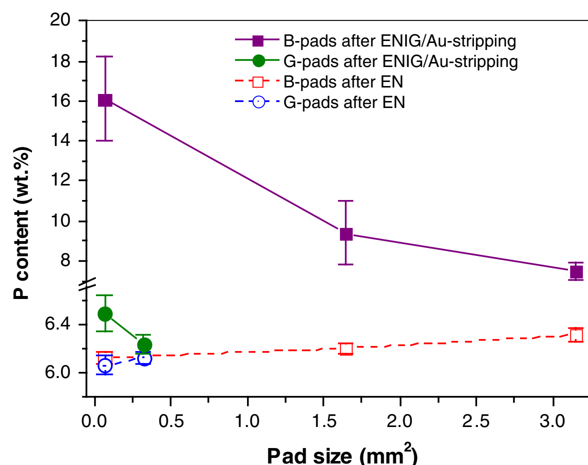

Fig. 10. Variation of P content as a function of pad size including pad connectivity before and after immersion gold processes.

Pad Area and Connectivity

Figure 10 shows the variation in P content with pad area and connectivity to a large pad (54.3 mm^2), measured by EPMA. Before the IG processes, the P content in each pad was not very different to each other and was in the range 6.06 wt.% to 6.31 wt.%. The P content in the Ni layers increased slightly to 8.5 wt.% in the G-pads after the ENIG processes. No clear dependence on the pad area was observed. However, the P content in the B-pads surprisingly increased to an average value of 16.08 wt.%. Considering pad connectivity, a strong dependence on pad area was observed: the smaller the pad size, the higher the P content in the bonding pad. The B-pads were connected to the large pad on the opposite side of a PCB. The B1 pad was the smallest pad in the experimental PCB testing with the same size as the G1 pad. The dependence of the P content on pad size when connected to the large pad is demonstrated for the first time in this paper. The large pad is around 830 times larger than the B1 pad, which can help us to understand why the tendency for corrosion in the Ni layers differed with location on the PCB. The bonding pads without any connection to the large pad have a greater possibility of corrosion resistance than those with the connection.

DISCUSSION

Terminology Describing Surface Defects

Surface defects exist as voids or black spikes in the Au layers. Since such corrosion voids are created

at the nickel/gold interfaces, the bonding strength between the solder balls and solder pads or bonding wires and wire pads is weakened, which results in bonding or soldering failure. Corroded surface defects of the nickel plating layers are widely known as black pad defects. In this paper, however, two different surface defect phenomena are reported: black pad and pinhole pad defects. As explained in the section “Defect Description”, these surface defect types depend on the thickness of the Au layers. There is a higher possibility of Ni diffusion into the Au surfaces in thin Au layers than in thick Au layers. The defect microstructures and defect characteristics, shown in Figs. 5 and 6, are almost identical for both defects. This indicates that, even if the phenomena revealed after ENIG are different, the origin of the surface defects is barely different. As a result, a change in the terminology of the black pad defects, meaning surface discoloring, would be suggested. Based on the observational results, the term “hypercorrosion defect” could be recommended.

Concentration Cell Corrosion

Figure 11 shows a schematic diagram showing immersion Au plating onto the PCB in a gold cyanide bath.

In the plating processes, the plating features can be schematically presented as shown in Fig. 12. At any given time, Ni atoms may be ionized and replaced by Au atoms. When it is assumed that there is no circulation of $Au(CN)_2^-$ ion solution in the bath, Ni ions may temporarily accumulate on the surfaces. This is likely to cause an unbalance of the Ni ion concentration in the bath. Thus concentration cell corrosion may be formed due to the difference in the metal ion concentration within the electrolyte,[13,14] as shown in Fig. 12. This cell can cause pits to form on the anodic pad. In the concentration cell assumed as above, a small pad, like the B1 pad connected to the large pad, may play the role of an anodic pad. As a result, surface defects such as the black pad or pinhole pad defects are more likely to be generated. Based on this model, the effect of pad size on corrosion can be understood.

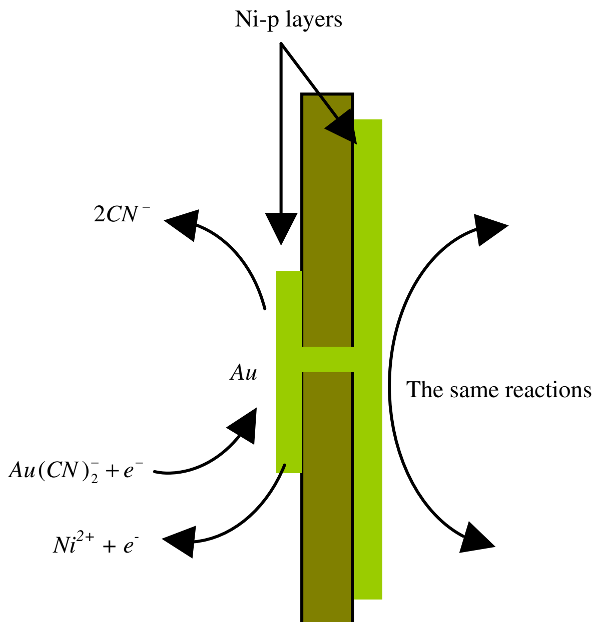

Fig. 11. Schematic diagram showing immersion Au plating in a gold cyanide bath.

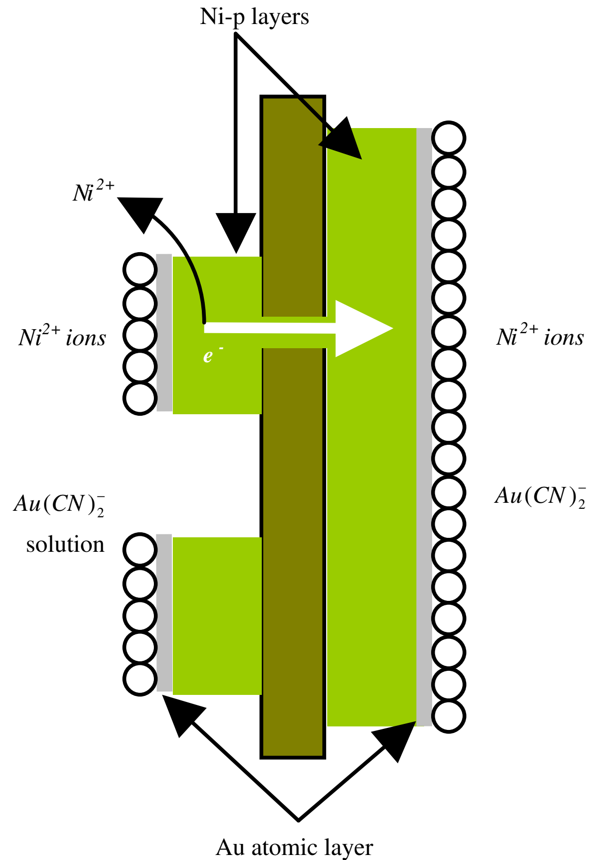

Fig. 12. Schematic diagram demonstrating the concentration cell corrosion model.

This model explains why the defect mode generated differs with pad position within a PCB. In fact, it has been pointed out that black pad defects do not take place in an irregular manner.[6]

It has been clearly emphasized that hypercorrosion does not occur randomly on electroless nickel surfaces; a high number of defects clustered on a few pads is observed. This evidence supports the proposed concentration cell corrosion model. In the previous report, it was proposed that a charge build up is responsible for the hypercorrosion triggered at nodule boundaries. However, this is not as clear and may be a misunderstanding. There is no further explanation for the charge build-up mechanism. If charges are generated and build up on the surfaces, they must build up on the sharpened area, such as nodule apexes, instead of the nodule spike area.

This unique model may not be independently working in all surface defects of the PCB pads.

There are several cases of pinhole pad defects, in samples belonging to G-pads, found without soldering and bonding failures.

Galvanic Cell Corrosion

In the pads where concentration cell corrosion is not likely to be expected, tiny dark spikes are also occasionally found. Therefore, a model capable of explaining these phenomena is required. If it is assumed that the Au lateral growth is slow or that the gold ion concentration is not homogeneous at the nodule boundaries, a hole or crevice along the nodule boundaries or nodule junctions can be generated. The reason for this is that the Au grain growth rate is relatively slow at the nodule boundaries or junctions compared to other sites within a pad. A stagnant zone will be formed at these sites. When these assumptions are correct, a galvanic cell can be formed as shown in Fig. 13. The following conditions for galvanic corrosion are generally required: (1) dissimilar metals, (2) electrical contacts between two different metals, and (3) a corrosive solution in contact with two metals.[13,14] The model proposed in Fig. 13 can satisfy these requirements. As a result, galvanic cell corrosion may take place at nodule boundaries or junctions of PCB pads. To support this model, the evidence of void formation at the boundaries or junctions should be examined at the initial stage. The lateral growth kinetics of the Au layer or an inhomogeneous Au solution at these positions within the bath should also be addressed.

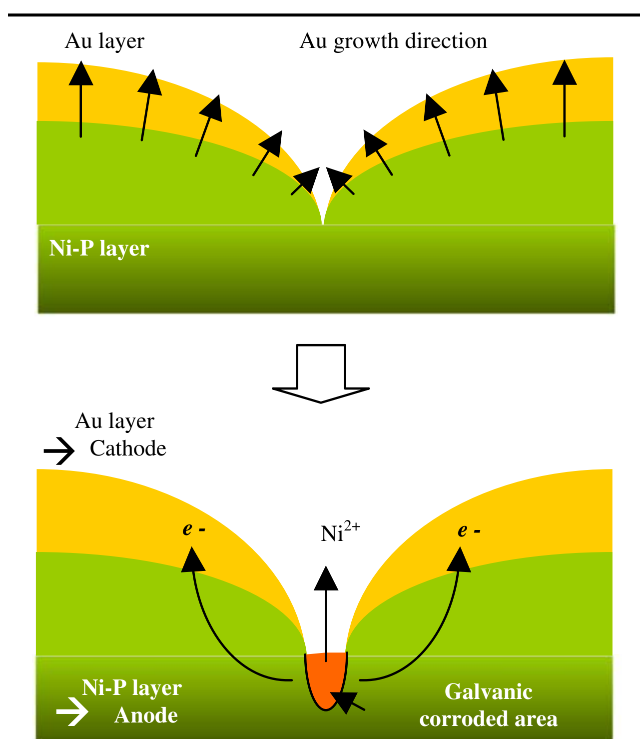

Fig. 13. Schematic diagram demonstrating the galvanic cell corrosion model.

Many researchers have claimed that galvanic corrosion takes place between the Ni layers and the Au ion solution bath, or due to the depletion of oxygen.[1,5,6] However, there is no explanation of where this galvanic corrosion occurred. The model suggested herein is therefore more realistic in terms of the detailed description of the corrosion cell.

Root Causes for Surface Defects

The mechanism for generating surface defects is likely to be explained by using the two models suggested above. A corrosion mechanism for surface defects, such as black pad or pinhole pad defects, is proposed involving concentration cell corrosion and galvanic cell corrosion. Based on these two models, the root causes for surface defects can be suggested as follows: Ni ion localization and inhomogeneous Ni ion concentration on the pads during the IG processes and the nodule morphology in the Ni layers before IG processes. To control these factors, it is necessary to investigate how the experimental parameters can affect these factors. These experiments are currently ongoing.

CONCLUSION

After the ENIG processes, surface defects affecting bondability or solderability failures are characterized. Based on the results obtained from these key findings, such as the surface defect microstructures and the P-content variation after the immersion gold plating, the following conclusions can be drawn.

(1) The hypercorrosion defects appear as two types of surface defects: black pad defects and pinhole pad defects. These two types of surface defects originate from the same root causes.
(2) The type of surface defect is determined by the Au thickness.
(3) From the variation of the P content detected on the Ni-P layers after ENIG, the degree of hypercorrosion can be estimated. The hypercorrosion defects are generated at the nodule boundaries or junctions of the Ni-P layers during the immersion gold plating processes. The P-content is up to 2.5 times higher in defective pads than in nondefective pads.
(4) Connectivity from small to large pads determines where surface defects are generated even if the pad sizes are approximately the same.
(5) A surface defect mechanism capable of explaining these hypercorrosion defects can be suggested based on a mixed corrosion mode of concentration cell corrosion and galvanic cell corrosion.

ACKNOWLEDGEMENT

The authors would like to thank the Analytical Engineering Group at SAIT and Dr. Baek, H.S. for their support of the FIB micrography work.

REFERENCES

1. K. Zeng, R. Stierman, D. Abbott, and M. Murtuza, *JOM* 58(6), 75 (2006).
2. K. Johal, S. Lamprecht, and H. Roberts, *SMTA Pan-Pacific Microelectronics Symposium*, 2004-atotech.com.
3. B. Houghton, *Proceedings of IPC Works 99, Session 4-3* (Minneapolis, MN, October 1999), pp. 1–9.
4. F. Cordes and R. Huemoeller, *IPC Printed Circuit Expo Conference Proceeding, Session 13-1* (Long Beach, CA, March 1999), pp. 1–6.
5. R.W.M. Kwok, K.C.M. Chan, and M.W. Bayes, *Circuit World* 30(4), 37 (2004).
6. N. Biunno, and M. Barbetta, *IPC Printed Circuit Expo Conference Proceeding, Session 18-5* (Long Beach, CA, March 1999), pp. 1–8.
7. D.J. Lee and H.S. Lee, *Microelectron. Reliab.* 46, 1119 (2006).
8. J.A. Roepsch, R.F. Champaign, and B.M. Waller, *SMTA International Conference Proceedings* (2003), pp. 404–411.
9. P. Snugovsky, P. Arrowsmith, and M. Romansky, *J. Electron. Mater.* 30(9), 1262 (2001).
10. R.A. Bulwith, M. Trosky, L.M. Picchione, and D. Hug, *Global SMT & Packaging* 2, 9 (2002).
11. K. Crouse and D. Cullen, PC FAB, Issue 2 (2002), pp. 22–32.
12. M. Walsh, CircuitTree, January (2001), pp. 10–16.
13. M.G. Fontana, *Corrosion Engineering*, 3rd ed., McGraw-Hill Series in Materials Science and Engineering (McGraw-Hill Book Company, 1986).
14. J.F. Shackelford, *Introduction to Materials Science for Engineers*, 2nd ed. (Macmillan Publishing Company, 1990).